Synthesis and thermal stability of ZnO nanowires

Madeha Ahmed Awad, Eslam Mohamed Mohamed Ibrahim & Ahmed Mohamed Ahmed

Journal of Thermal Analysis and Calorimetry
An International Forum for Thermal Studies

ISSN 1388-6150
Volume 117
Number 2

J Therm Anal Calorim (2014)
117:635-642
DOI 10.1007/s10973-014-3836-x

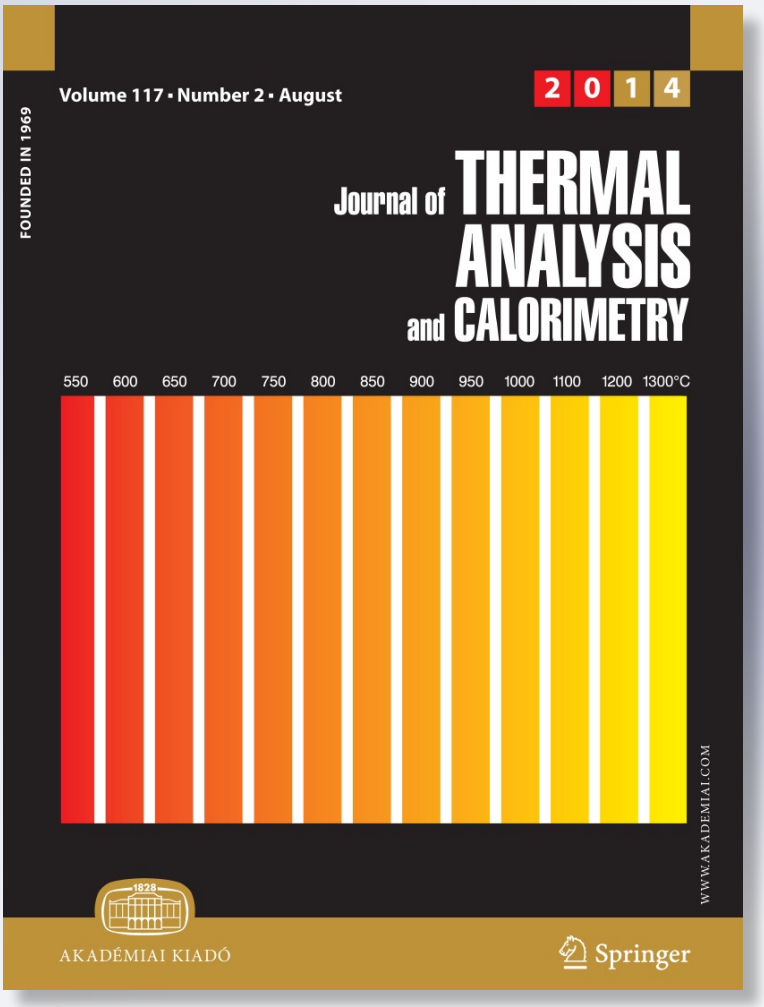

Springer

J Therm Anal Calorim (2014) 117:635–642
DOI 10.1007/s10973-014-3836-x

Synthesis and thermal stability of ZnO nanowires

Madeha Ahmed Awad · Eslam Mohamed Mohamed Ibrahim · Ahmed Mohamed Ahmed

Received: 16 November 2013 / Accepted: 22 April 2014 / Published online: 31 May 2014

Abstract ZnO nanowires (NWs) were synthesized on Au-coated Si (100) substrates by vapor transport method. The effect of high temperature annealing on the structural and chemical composition as well as thermal stability was studied. The as-prepared ZnO NWs was nearly stoichiometric and identified as hexagonal ZnO phase. After annealing at 1,473 K, the atomic ratio of O/Zn, the intensity of the diffraction peaks, and the diameter of nanowires were increased. The ZnO NWs were fragmented into nanocrystals and the fragments coalesced with each other after annealing at 1,673 K. The thermal stability of ZnO NWs was studied by thermo-gravimetric (TG) analysis. A sharp increase in the TG curves was observed and can be attributed to the oxidation of some possibly presented Zn atoms. The activation energy of oxidation of Zn interstitial atoms was found to be 484.81 kJ mol^{-1}. A mass gain peak was observed after annealing at 1,473 K, but it was completely eliminated after annealing at 1,673 K.

Keywords ZnO NWs · Vapor transport · Annealing · Thermal stability

Introduction

ZnO nanomorphologies are extensively investigated due to ease of synthesis, excellent control over morphology, and excellent optical and electrical properties [1–4]. In particular, ZnO one-dimensional (1D) nanostructures are attractive material platform for chemical and biological sensors [5, 6], field-emission materials [7], self-powered photodetectors [8], dye-sensitized solar cells [9], piezoelectric [10], and thermoelectric devices [11].

ZnO 1D nanostructures can be synthesized by several techniques including vapor processes using metal organic chemical vapor deposition (MOCVD) [12], magnetron sputtering [13], pulsed laser deposition [14], as well as wet chemical processes, such as hydrothermal decomposition [15] and electrochemical reaction [16]. The most employed vapor process method is the vapor transport technique, where zinc or zinc oxide powder is evaporated in the middle of a horizontal tube furnace heated at 873–1,323 K [5, 7, 17–21]. The vapor is then carried by gas stream and condenses forming the nanostructures. The growth parameters, such as the temperature of the feedstock and substrates, pressure, catalyst, gas flow rate, and oxygen content can be adjusted to grow the structures of interest. The growth process typically takes from 15 to 60 min.

Many device fabrication processes involve high temperature annealing (dopant activation, ohmic contact formation, implantation repairs), so the effect of temperature on the properties of the NWs is crucial to the realization of nanodevices based on ZnO NWs [18]. Annealing can improve the field-emission (FE) characteristics of ZnO NWs [22]. Additionally, the stability at higher temperatures is a request for the application of ZnO NWs as oxygen gas sensor which usually operates at high temperatures [23]. Therefore, in this article we have reported on the synthesis of ZnO NWs using vapor transport technique. The effect of high temperature annealing on the chemical and structural properties of ZnO NWs has been investigated. In addition, the thermal stability of ZnO NWs has been also studied by thermo-gravimetric analysis.

M. A. Awad (✉) · E. M. M. Ibrahim · A. M. Ahmed
Physics Department, Faculty of Science, Sohag University, Sohag 82524, Egypt
e-mail: arwamadeha@yahoo.com

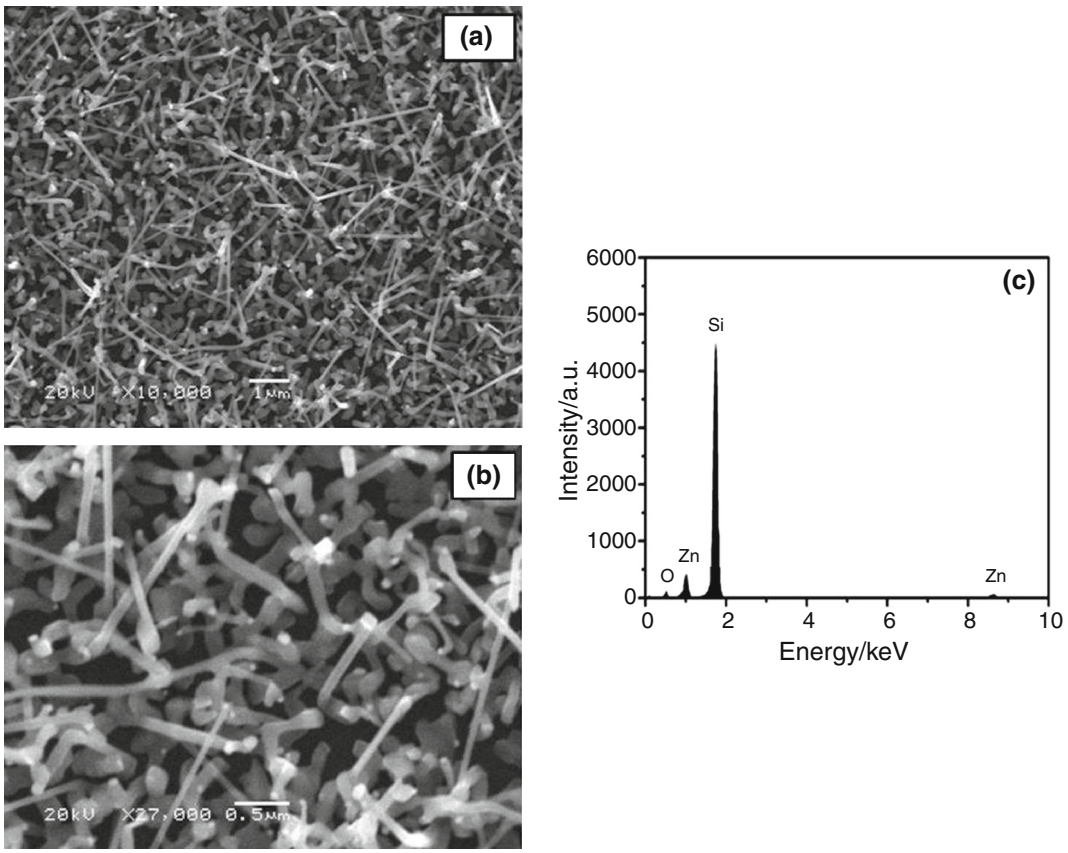

Fig. 1 SEM images of as-prepared ZnO NWs grown on Si substrate with low (**a**) and high (**b**) magnifications. (**c**) EDAX spectrum of as-prepared ZnO NWs grown on Si substrate

Experimental

ZnO nanostructures were synthesized by thermal evaporation method with vapor–liquid–solid (VLS) growth technique where Zn metal granules, ~2 mm diameter (Aldrich chemicals; 99.95 %), were placed at 1,173 K in an alumina boat at the center of the quartz tube furnace (internal diameter 3.6 cm and length of 60 cm). The synthesis was carried out on Au-coated (~25–30 nm) Si (100) wafers (cut into 1 cm × 1 cm and ultrasonically cleaned). The substrates were coated using AC Ion sputtering device (JFC-1100E), Mixture of high-purity argon and oxygen gases was flowed into the tube furnace at flow rates 200 and 20 sccm, respectively, to push the gaseous precursors from the furnace center to deposit on the substrates. The time of deposition was 30 min. After deposition, the furnace was cooled down to room temperature, and some of the deposited material was scratched from the Au-coated Si (100) substrates. Subsequently, some samples were separately annealed in air at 1,473 and 1,673 K for 60 min, respectively, to investigate the changes in the crystalline structure and morphology.

The surface morphology and crystal structure of the synthesized nanostructures were characterized by scanning electron microscope SEM (type JOEL model JSM-6380 LA) and X-ray diffraction XRD (type Shimadzu Diffractometer XRD 6000, which utilizing CuK_α radiation ($\lambda = 1.54056$ Å), respectively. The chemical composition of the synthesized nanostructures was analyzed using energy dispersive analysis of X-ray (EDAX) unit attached with the SEM. The powder scratched out of the substrate was used for thermo-gravimetric analysis (TG) measurement (with heating rates = 5, 10, 20, 30, and 40 K min^{-1}). The TG measurements were carried out using Shimadzu DTG-60AH Thermo-gravimetric Analyzer. The samples (mass app. 2.7 mg) were heated in a standard platinum pan from room temperature to 1,773 K.

Results and discussion

SEM and EDAX for as-prepared and annealed samples

The morphologies of the as grown ZnO nanostructures on Au-coated Si substrates with low and high magnifications

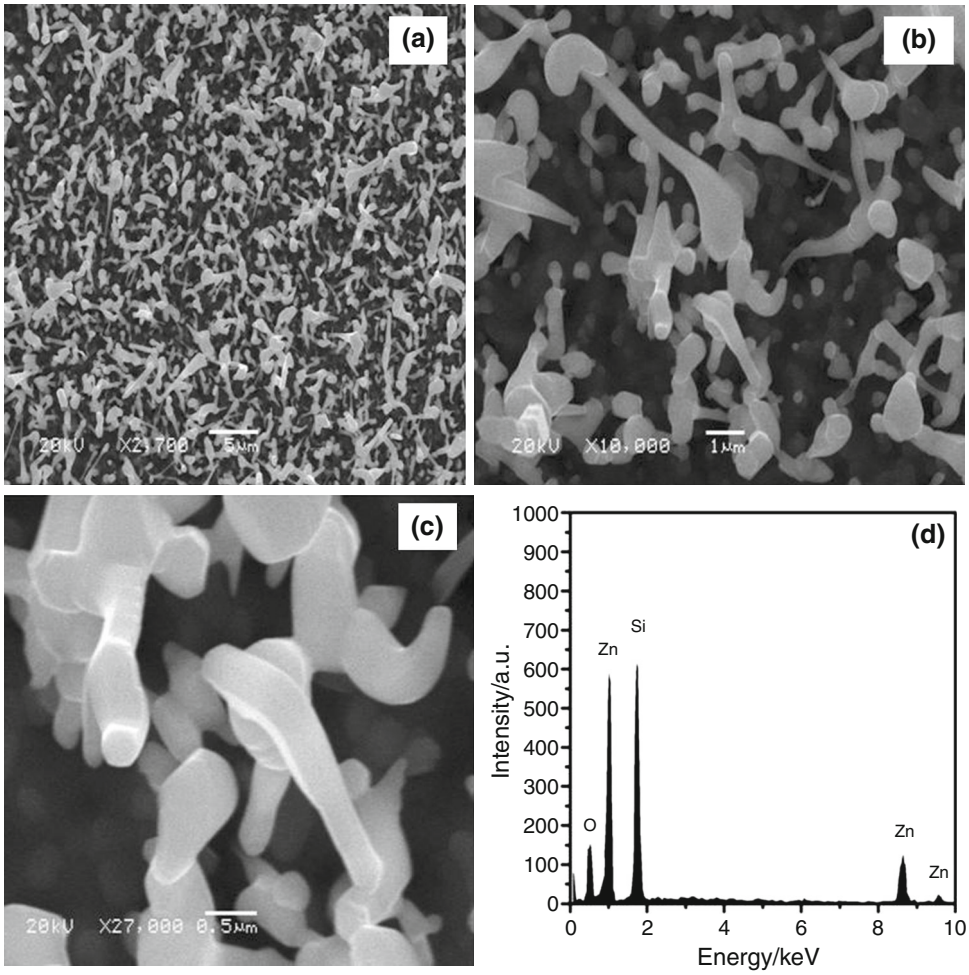

Fig. 2 SEM images of ZnO NWs annealed at 1,473 K with low (**a**), (**b**) and high (**c**) magnifications. (**d**) EDAX spectrum of ZnO NWs grown on Si substrate and annealed at 1,473 K

are shown in Fig. 1a, b. The data reveal that products are nanowires, randomly oriented on the Si substrate, including some nanoparticles. The SEM investigations allow determining the diameter and length of nanowires, which were found to be in ranges of 65–146 nm and 0.8–2.1 μm, respectively. The growth mechanism of ZnO nanowires may proceed via the following steps. The oxygen/argon gas-mixture stream transports Zn vapor from the molten feedstock to the substrate. The next stage is the impingement of the precursors from the gas phase on the substrate, then effectively condensation of the precursors and nanostructure nucleation. During the growth process and due to the high temperature, Au islands can melt into Au liquid droplets (dots) and then they are able to capture the volatiles transported by the gas stream forming a eutectic alloy. Precipitation of Zn occurs when the supersaturation is reached, and the nanowires originate from the liquid Au-catalytic droplets. The nanowires continue to grow by the vapor–liquid–solid (VLS) mechanism [19, 24, 25]. Formation of the ZnO nanoparticles may be ascribed to the long deposition time (30 min) where all Au-catalyst was exhausted in forming nanowires after a period of time and thus the incoming volatile precipitate among nanowires in the form of ZnO nanoparticles.

The chemical composition of the as-synthesized ZnO nanostructure characterized by the EDAX is shown in Fig. 1c. It is found that the nanostructure mainly composed of Zn and O. The observed Si peak originates from the Si (100) substrate. The atomic percents of Zn and O elements are 52.12 ± 2 and 47.78 ± 2 at %, respectively. Noteworthy, different positions of ZnO nanostructure were examined and show almost the same ratio of O/Zn. This confirms that the prepared ZnO is nearly stoichiometric.

SEM images for the sample annealed at 1,473 K, with low and high magnifications, are shown in Fig. 2a–c. Obviously, the shape of the wires is significantly deformed. The deformation is accompanied with the increase in diameter and length of the nanowires , which are found to be in the ranges of 359–620 nm and 1.1–2.4 μm, respectively. The EDAX spectrum of the sample annealed at

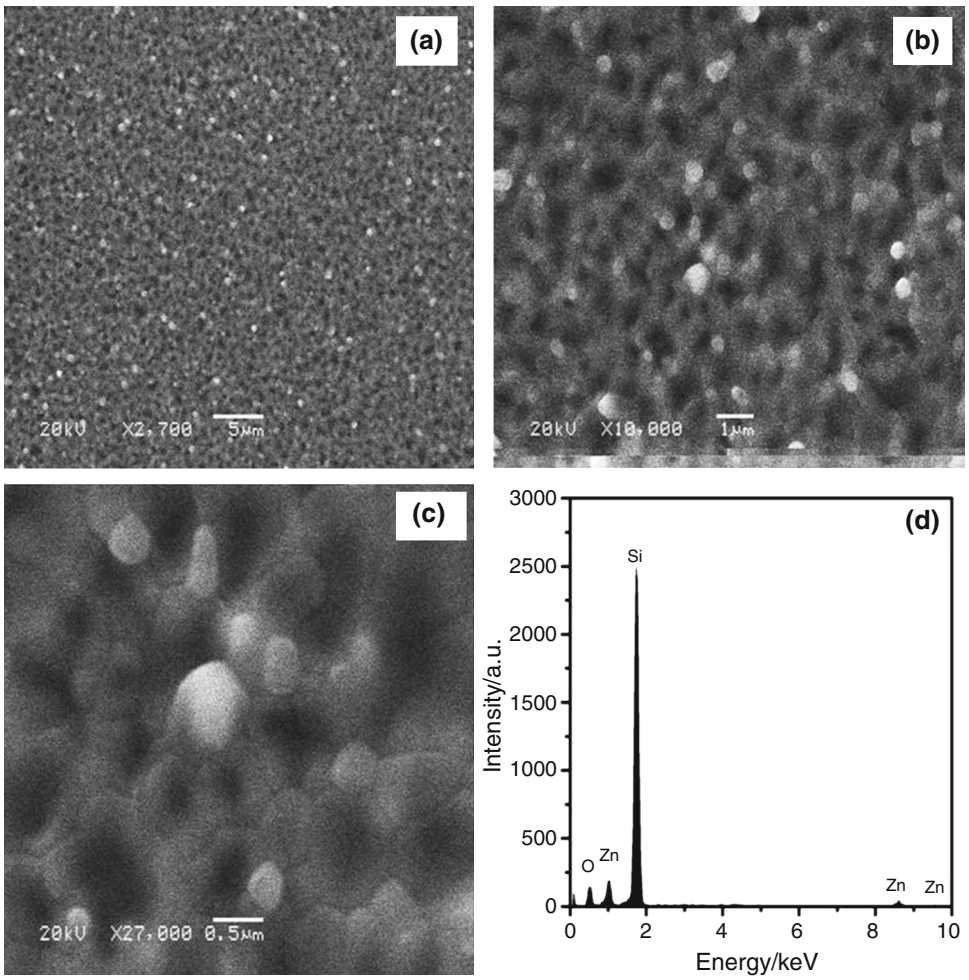

Fig. 3 SEM images of ZnO NWs annealed at 1,673 K with low (**a**), (**b**) and high (**c**) magnifications. (**d**) EDAX spectrum of ZnO NWs grown on Si substrate and annealed at 1,673 K

1,473 K is depicted in Fig. 2d. The atomic percentages of Zn and O are 49.13 at % and 50.87 at %, respectively, which indicates that the oxygen ratio increased upon annealing at 1,473 K.

Figure 3a–c shows SEM images for samples annealed at 1,673 K. The images illustrate that the 1D ZnO NWs transformed to 0D nanoparticles and they coalesced together so that it is difficult to distinguish individual nanoparticles. The coalescence may occur through atomic diffusion and rearrangement which are effectively accelerated due to large surface area of nanowires [26, 27]. The EDAX analysis of the sample annealed at 1,673 K (Fig. 3d) reveals atomic percentages of Zn and O elements as 39.82 at. % 60.18 at. %, respectively. This implies a reduction of Zn element and present of an over stoichiometric of oxygen. The reduction of Zn element upon annealing has been observed previously by Kim et al. [28] for ZnO/SiOx core–shell nanowires annealed at 1,173-1,273 K.

XRD examinations for as-prepared and annealed ZnO NWs

Figure 4a–c shows XRD patterns of the as-prepared and annealed ZnO NWs. All the diffraction peaks can be identified as hexagonal ZnO structure (JCPDS file no.79-0208) with lattice constants of $a = 3.27$ Å and $c = 5.20$ Å. No diffraction peaks of pure Zn phase or other impurities can be observed confirming that the sample crystallizes in single ZnO phase [29]. Noteworthy, the crystal orientation was found to be significantly dependent on the annealing temperature. To be specific, the intensities of the induced peaks (except that of the (004) peak) increase by annealing at 1,473 K and the peaks shift about (0.04°) toward higher 2θ. After annealing at 1,673 K, the intensity of the peaks (002), (101), (102), (103), and (112) significantly increases which indicates that the orientation of the ZnO nanocrystals in these directions is favorable [30, 31]. The XRD peaks of the sample annealed at

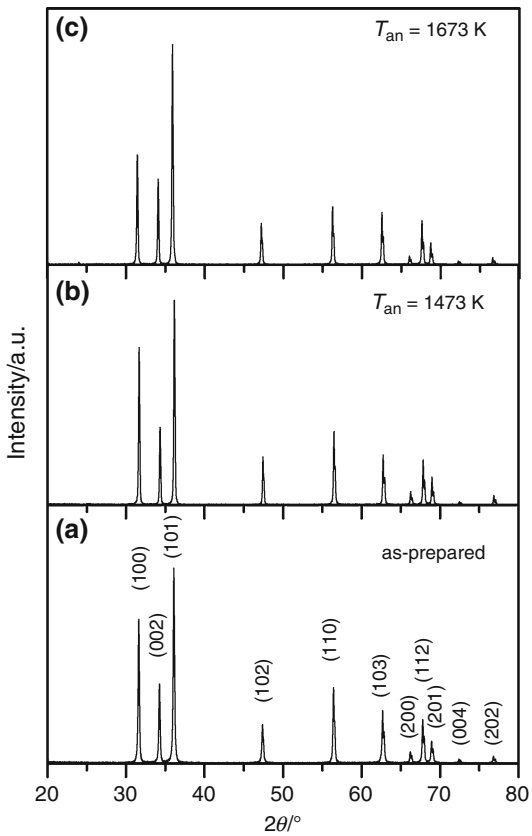

Fig. 4 XRD patterns of as-prepared ZnO NWs (**a**), annealed at 1,473 K (**b**) and annealed at 1,673 K (**c**)

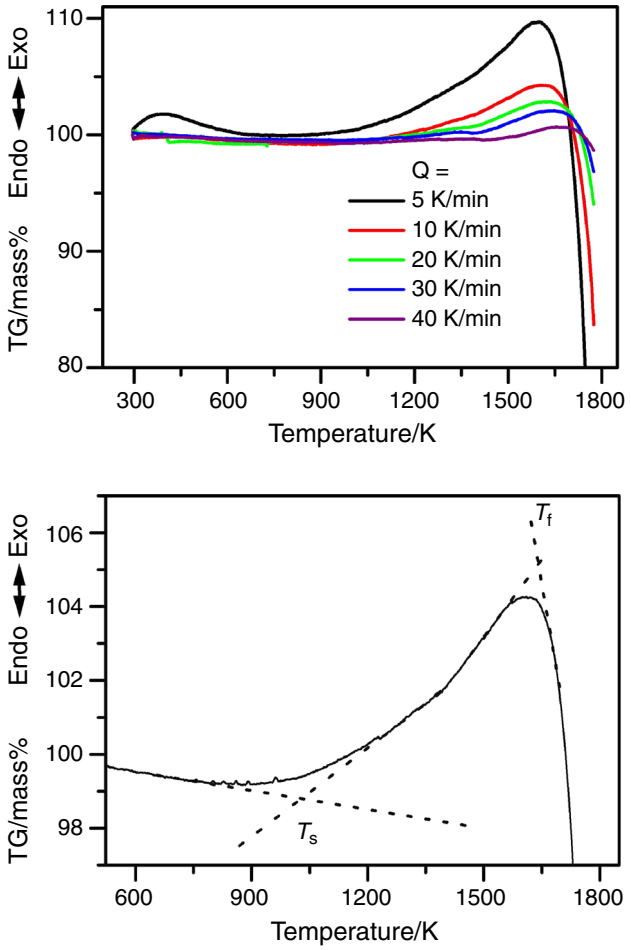

Fig. 6 TG curves at different heating rates (Q = 5, 10, 20, 30 and 40 K min^{-1}) of as-prepared ZnO NWs powders

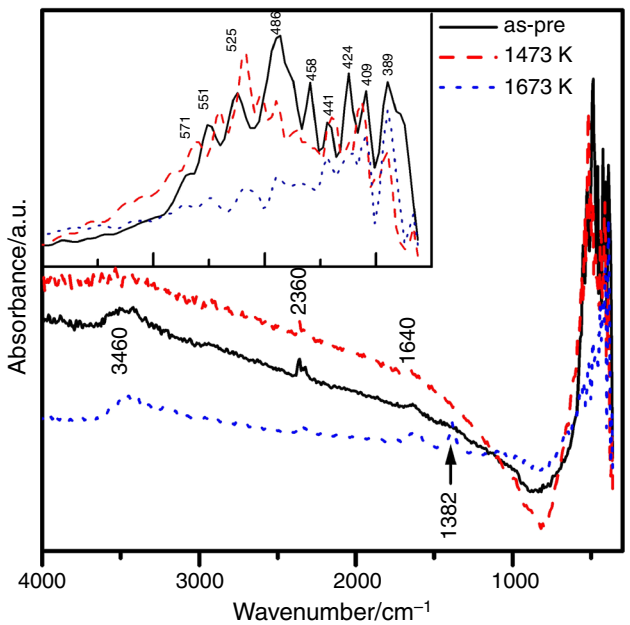

Fig. 5 FTIR spectra of as-prepared and annealed ZnO nanostructures

Table 1 Calculated values of T_s/K and T_f/K at different heating rates

Q/K min^{-1}	T_s/K	T_f/K
5	951.2	1598.5
10	1210.2	1620.4
20	1293.6	1651.1
30	1325.4	1670.1
40	1428.8	1689.3

1,673 K show a shift of 0.22° toward lower 2θ as compared with those of the as-prepared sample ZnO. The lattice constants of the sample annealed at 1,673 K are a = 3.28 Å and c = 5.23 Å. Palni et al. [32] examined the effect of the post deposition annealing on the ZnO NWs. They observed that the diffraction peak intensities increased, the peaks became narrower and the crystallinity of the NWs significantly improved. They attributed this to the increase in the average diameter of the nanowires and reduction in the strain, as a result of heat treatment. Similar observations have been reported by Manzoor and Kim [33],

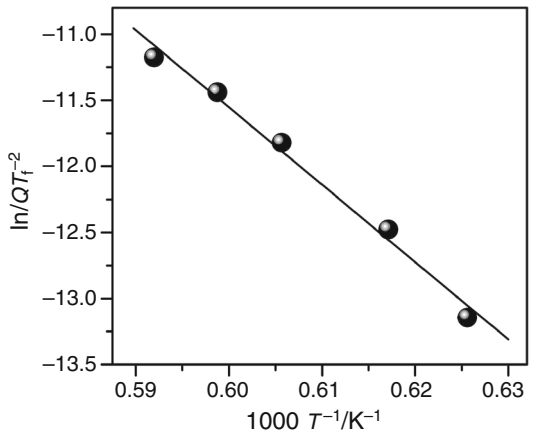

Fig. 7 $\ln(QT_f^{-2})$ versus 1000 T_f^{-1} plot

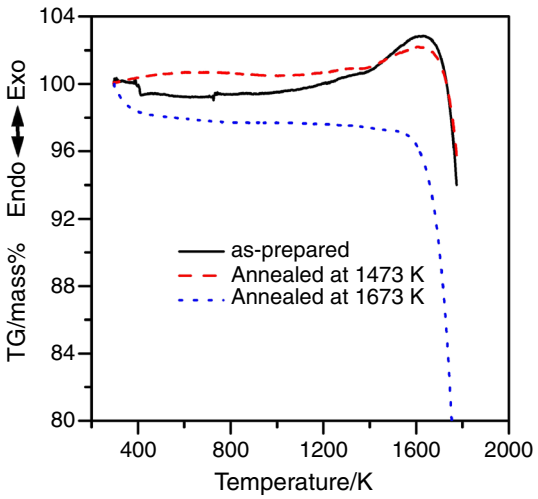

Fig. 8 TG curves as a function of temperature for as-prepared and annealed powder samples at 1,473 K and 1,673 K (for 60 min). the heating rate $Q = 20$ K min^{-1}

and Mekasuwandumrong et al. [34] for post-annealed ZnO nanocombs and ZnO nanoparticles, respectively.

FTIR analysis

Inside any material, there are different bonds vibrate with different frequencies, so they can absorb different frequencies of the IR light. When a frequency of the IR light resonates with the frequency of particular vibrational mode, the IR light will be absorbed causing stretching or bend increasing of the bonds. The FTIR spectra of the as-synthesized and, annealed ZnO nanostructures at 1,473 and 1,673 K were recorded over the range of 300–4,000 cm^{-1} and depicted in Fig. 5. The broad absorption band around 3,460 cm^{-1} is due to the O–H stretching vibration of water molecules while the band at 1,640 cm^{-1} indicates –OH bending. The band at 2,360 cm^{-1} is due to the adsorbed atmospheric CO_2. The bands appear within the range of 600–350 cm^{-1} characterize the Zn–O bond and crystal lattice vibrations (see the inset of Fig. 5) [35–37]. In the case of the sample annealed at 1,473 K, there are slight changes in the positions and intensities of the absorption bands of the Zn–O bond. This indicates that annealing at 1,473 K has slight effect on the wurtzite structure of the ZnO as confirmed above from the XRD results. Upon annealing at 1,673 K, a new strong band appears around 1,382 cm^{-1} and a pronounced change in the absorption bands positions and intensities of the Zn–O bonds can be observed. The newly appearing band at 1,382 cm^{-1} may be ascribed to the chemical interaction of the ZnO surface with the oxygen of the C=O group because the annealing process of the FTIR was carried out in the ambient atmosphere. This confirms that the nature of the bonds is strongly affected by annealing at 1,673 K.

Thermo-gravimetric analysis (TG)

The TG curves recorded at different heating rates ($Q = 5$, 10, 20, 30, and 40 K min^{-1}) of the ZnO powder are shown in Fig. 6a. Clearly, the water and gases adsorbed in the sample and the crucible are removed below 873 K. In the analyses of our results, this part of the mass loss curve is ignored. The mass loss increases gradually with increasing temperature up to a certain value (T_s) beyond which a sharp increase starts to occur. This sharp increase is attributed to the oxidation of some possibly existed Zn atoms. It has been stated previously that the transition metals oxides prepared by the vapor transport method generally contain excess metal atoms in the interstitial positions of the oxide and cannot strictly reach the stoichiometry in normal conditions [19, 25, 38–40]. This is clearly seen from the presence of a sharp mass gain in the TG curve. After that the oxidation gradually slows down and a huge mass loss starts at certain temperature (T_f) denoting completion of the oxidation process. Here T_s and T_f are the onset and the end of oxidation, respectively, and are determined and listed in Table 1 using the well-known way shown in Fig. 6b. The values imply that they shift to higher temperatures as the heating rate increases.

To determine the activation energy, the peak temperature of the oxidation (T_f) at different heating rates (Q) was applied to Kissinger model:

$$\ln\left(\frac{Q}{T_f^2}\right) = -\frac{E_a}{RT_f} + \text{constant}, \quad (1)$$

where R is the universal gas constant, E_a is the activation energy. The kinetic parameter can be determined from graphs of the logarithm of Q divided by the square of

temperature that measured at the maximum of oxidation (T_f) versus the reciprocal of T_f as shown in Fig. 7. The activation energy is the minimum amount of energy required for oxidation. It was found that the value of E_a for ZnO NWs is 484.81 kJ mol^{-1}.

Thermal stability is the stability of a molecule at high temperatures, i.e., a molecule with more stability has more resistance to decompose at high temperatures [41–43]. The thermal stability of a system depends on its free energy, where the lower the free energy, the more stable is the system. Under normal conditions, wurtzite ZnO is thermodynamically stable. Figure 8 shows the TG curves measured at heating rate 20 K min^{-1} as a function of temperature for the as-prepared and annealed samples. The mass gain peak (oxidation peak) observed for the as-prepared sample still appears for the sample annealed at 1,473 K. This means that annealing in air at 1,473 K for 60 min is not sufficient for full oxidation of the all Zn atoms i.e., the sample still stable. However, the sample annealed at 1,673 K does not show any mass gain peak (oxidation peak), confirming that annealing in air at 1,673 K for 60 min is optimum condition for full oxidation of Zn atoms in the ZnO NWs.

Conclusions

Well-crystallized ZnO NWS were successfully synthesized by vapor transport method. The effect of annealing at higher temperatures on structural and compositional properties as well the morphology was investigated. Annealing at 1,473 K increases the intensity of the diffraction peaks and the diameter of the NWs. However, by annealing at 1,673 K, the 1D NWs transform to 0D nanoparticles which coalesced with each other. The TG plots revealed the presence of Zn interstitial atoms in the ZnO NWs that were not oxidized during growth in the system. The activation energy required for full oxidation of the Zn atoms was found to be 484.81 kJ mol^{-1} which can be realized by annealing at 1,673 K. Stability of the Zn interstitial atoms at high temperature confirms the feasibility of using the synthesized ZnO NWs as gas sensors at high temperatures.

References

1. Ramgir N, Datta N, Kaur M, Kailasaganapathi S, Debnath AK, Aswal DK, Gupta SK. Metal oxide nanowires for chemiresistive gas sensors: issues, challenges and prospects. Colloid Surf A. 2013;439:101–16.
2. Fan G, Huang Z, Jiang J, Sun L. Standard molar enthalpy of formation of the ZnO nanosheets. J Therm Anal Calorim. 2012;110:1471–4.
3. Rishikeshi SN, Joshi S. Cu–ZnO nanocrystallites by aqueous thermolysis method. J Therm Anal Calorim. 2012;109:1473–7.
4. Wang L, Ma Z, Liu S, Huang Z. In situ growth mechanism and the thermodynamic functions of zinc oxide nano-arrays and hierarchical structure. J Therm Anal Calorim. 2014;115:201–8.
5. Hwang I-S, Kim S-J, Choi J-K, Choi J, Ji H, Kim G-T, Cao G, Lee J-H. Synthesis and gas sensing characteristics of highly crystalline ZnO–SnO2 core–shell nanowires. Sens Actuator B. 2010;148:595-5.
6. Choi A, Kim K, Jung HJ, Lee SY. ZnO nanowire biosensors for detection of biomolecular interactions in enhancement mode. Sens Actuator B. 2010;148:577-6.
7. Mosquera E, Bernal J, Zarate RA, Mendoza F, Katiyar RS, Morell G. Growth and electron field-emission of single-crystalline ZnO nanowires. Mater Lett. 2013;93:326-4.
8. Hatch SM, Briscoe J, Sapelkin A, Gillin WP, Gilchrist JB, Ryan MP, Heutz S, Dunn S. Influence of anneal atmosphere on ZnO-nanorod photoluminescent and morphological properties with self-powered photodetector performance. J Appl Phys. 2013;113:204501–5.
9. Law M, Greene LE, Johnson JC, Saykally R, Yang PD. Nanowire dye-sensitized solar cells. Nat Mater. 2005;4:455-5.
10. Wang ZL, Song JH. Piezoelectric nanogenerators based on zinc oxide nanowire arrays. Science. 2006;312:242–5.
11. Shi LH, Chen J, Zhang G, Li BW. Thermoelectric figure of merit in Ga-doped [0001] ZnO nanowires. Phys Lett A. 2012;376:978-4.
12. Cabibbo M. Deep-cryogenic treatment of ZnO nanowires. Mater Lett. 2013;100:145-3.
13. El Mel A, Buffiere M, Massuyeau F, Gautron E, Xu W, Choi C-H, Wery J, Faulques E, Barreau N, Tessier P-Y. Direct synthesis of ZNO nanowires on nanopatterned surface by magnetron sputtering. Chem Vap Depos. 2011;17:337-5.
14. Lorenz M, Cao B, Zimmermann G, Biehne G, Czekalla, Frenzel H, Brandt M, von Wenckstern H, Grundmann M. Stable p-type ZnO: P nanowire/n-type ZnO:Ga film junctions, reproducibly grown by two-step pulsed laser deposition. Vac. Sci Technol B. 2009;27:1693–5.
15. Wang J-C, Liang Y-T, Cheng F-C, Fang C-H, Chen H-I, Tsai Ch-Y, Jiang J-A, Nee T-E. Enhancement of exciton radiative recombination for In-doped ZnO nanowires with aluminum cylindrical micropillars. J Lumin. 2013;136:11–6.
16. Leprince-Wang Y, Wang GY, Zhang XZ, Yu DP. Study on the microstructure and growth mechanism of electrochemical deposited ZnO nanowires. J Cryst Growth. 2006;287:89-5.
17. Hsu C-L, Chen K-C, Tsai T-Y, Hsueh T-J. Fabrication of gas sensor based on p-type ZnO nanoparticles and n-type ZnO nanowires. Sens Actuator B. 2013;182:190–7.
18. Maffeis TGG, Penny MW, Castaing A, Guy OJ, Wilks SP. XPS investigation of vacuum annealed vertically aligned ultralong ZnO nanowires. Surf Sci. 2012;606:99-5.
19. Mohamed SH. Synthesis, structural and ellipsometric evaluation of oxygen-deficient and nearly stoichiometric zinc oxide and indium oxide nanowires/nanoparticles. Phil Mag. 2011;91:3598-14.
20. Li X, Qi J, Zhang Q, Zhang Y. Temperature-dependent electron transport in ZnO micro/nanowires. J Appl Phys. 2012;112:084313–4.
21. Bae MY, Min KW, Yoon J, Kim G-T, Ha JS. Electronic properties of light-emitting p-n hetero-junction array consisting of p + -Si and aligned n-ZnO nanowires. J Appl Phys. 2013;113:084310–5.
22. Wang J-L, Hsieh T-Y, Yang P-Y, Hwang C–C, Shye D-C, Lee I-C. Oxygen annealing effect on field-emission characteristics of hydrothermally synthesized Al-doped ZnO nanowires. Surf Coat Technol. 2013;231:423–5.

23. Lu C-Y, Chang S-P, Chang S-J, Hsueh T-J, Hsu C-L, Chiou Y-Z, Chen I-C. ZnO nanowire-based oxygen gas sensor. IEEE Sens J. 2009;9:485-5.
24. Saunders RB, McGlynn E, Biswas M, Henry MO. Thermodynamic aspects of the gas atmosphere and growth mechanism in carbothermal vapour phase transport synthesis of ZnO nanostructures. Thin Solid Films. 2010;518:4578-4.
25. Mohamed SH, El-Hagary M, Althoyaib S. Growth of β-Ga2O3 nanowires and their photocatalytic and optical properties using Pt as a catalyst. J Alloys Compd. 2012;537:291–6.
26. Sun SB, Zhao YM, Xia YD, Zou ZD, Min GH, Zhu YQ. Bundled tungsten oxide nanowires under thermal processing. Nanotechnology. 2008;19:305709-7.
27. QinY, Shen W, Li X, Hu M. Effect of annealing on microstructure and NO2-sensing properties of tungsten oxide nanowires synthesized by solvothermal method. Sens Actuator B. 2011;155: 646–7.
28. Kim HW, Kebede MA, Kim HS, Kong MH, Lee C. Effects of annealing on the structure and photoluminescence of ZnO-sputtered coaxial nanowires. J Lumin. 2009;129:1619-6.
29. Ibrahim EMM. The effect of sintering time and temperature on the electrical properties of MnZn ferrites. Appl Phys A. 2007;89:203–6.
30. Saleh SA, Khalil SM, Ibrahim EMM. Influence of sintering temperature on thermopower and hardness of RuSr2GdCu2O8. Supercond Sci Technol. 2007;20:372–5.
31. Ibrahim MM, Ibrahim EMM, Saleh SA, Hakeem AMA. Synthesis and characterization of semi magnetic semiconductor Pb1-xSmxSe. J Alloys Compod. 2007;429:19–24.
32. Palni PP, Kumari S, Baruah NG, Singh DK, Giri PK. Effect of annealing on high quality zinc oxide nanowires synthesized by catalytic vapor-deposition. Nano Trends: J Nanotechnol Appl. 2007;3:1–6.
33. Manzoor U, Kim DK. Size control of ZnO nanostructures formed in different temperature zones by varying Ar flow rate with tunable optical properties. Physica E. 2009;41:500–6.
34. Mekasuwandumrong O, Pawinrat P, Praserthdam P, Panpranot J. Effects of synthesis conditions and annealing post-treatment on the photocatalytic activities of ZnO nanoparticles in the degradation of methylene blue dye. Chem Eng J. 2010;164:77–8.
35. Lanje AS, Sharma SJ, Ningthoujam RS, Ahn J-S, Pode RB. Low temperature dielectric studies of zinc oxide (ZnO) nanoparticles prepared by precipitation method. Adv Powder Technol. 2013;24: 331–5.
36. Stambolova I, Blaskov V, Shipochka M, Vassilev S, Petkova V, Loukanov A. Simple way for preparation of ZnO films by surfactant mediated spray pyrolysis. Mater Sci Eng, B. 2012;177:1029-9.
37. Khan Y, Durrani SK, Mehmood M, Ahmad J, Khan MR, Firdous S. Low temperature synthesis of fluorescent ZnO nanoparticles. Appl Surf Sci. 2010;257:1756-6.
38. Choi JS, Yo CH. Study of the nonstoichiometric composition of zinc oxide. J Phys Chem Solids. 1976;37:1149-3.
39. Lupan O, Emelchenko GA, Ursaki VV, Chai G, Redkin AN, Gruzintsev AN, Tiginyanu IM, Chow L, Ono LK, Cuenya BR, Heinrich H, Yakimov EE. Synthesis and characterization of ZnO nanowires for nanosensor applications. Mater Res Bull. 2010; 45:1026–7.
40. Mohamed SH. SnO2 dendrites–nanowires for optoelectronic and gas sensing applications. J Alloy Compd. 2012;510:119-6.
41. Zhou ZF, Pan Y, Zhou YC, Yang L. Growth dynamics and thermal stability of Ni nanocrystalline nanowires. Appl Surf Sci. 2011;257:9991–5.
42. Ibrahim EMM, Hampel S, Kamsanipally R, Thomas J, Erdmann K, Susanne F, Taeschner C, Khavrus VO, Gemming T, Leonhardt A, Buechner B. Highly biocompatible superparamagnetic Ni nanoparticles dispersed in submicron-sized C spheres. Carbon. 2013;63:358–9.
43. Ibrahim EMM, Hampel S, Wolter AUB, Kath M, El-Gendy AA, Klingeler R, Taeschner C, Khavrus VO, Thomas G, Leonhardt A, Buechner B. Superparamagnetic FeCo and FeNi Nanocomposites Dispersed in Submicrometer-Sized C Spheres. J Phys Chem C. 2012;116:22509-9.